INTERNATIONAL JOURNAL OF ENERGY RESEARCH
Int. J. Energy Res. 2002; **26**:893–920 (DOI: 10.1002/er.827)

On the effect of the local turbulence scales on the mixing rate of diffusion flames: assessment of two different combustion models

Jose Lopes[‡], Viriato Semião*[,†,§] and Maria da Graça Carvalho[¶]

Instituto Superior Tecnico, Mechanical Engineering Department, Av. Rovisco Pais, 1049-001 Lisboa, Portugal

SUMMARY

A mathematical model for the prediction of the turbulent flow, diffusion combustion process, heat transfer including thermal radiation and pollutants formation inside combustion chambers is described. In order to validate the model the results are compared herein against experimental data available in the open literature. The model comprises differential transport equations governing the above-mentioned phenomena, resulting from the mathematical and physical modelling, which are solved by the control volume formulation technique. The results yielded by the two different turbulent-mixing physical models used for combustion, the simple chemical reacting system (SCRS) and the eddy break-up (EBU), are analysed so that the need to make recourse to local turbulent scales to evaluate the reactants' mixing rate is assessed. Predictions are performed for a gaseous-fuelled combustor fired with two different burners that induce different aerodynamic conditions inside the combustion chamber. One of the burners has a typical geometry of that used in gaseous fired boilers—fuel firing in the centre surrounded by concentric oxidant firing—while the other burner introduces the air into the combustor through two different swirling concentric streams. Generally, the results exhibit a good agreement with the experimental values. Also, NO predictions are performed by a prompt-NO formation model used as a post-processor together with a thermal-NO formation model, the results being generally in good agreement with the experimental values. The predictions revealed that the mixture between the reactants occurred very close to the burner and almost instantaneously, that is, immediately after the fuel-containing eddies came into contact with the oxidant-containing eddies. As a result, away from the burner, the SCRS model, that assumes an infinitely fast mixing rate, appeared to be as accurate as the EBU model for the present predictions. Closer to the burner, the EBU model, that establishes the reactants mixing rate as a function of the local turbulent scales, yielded slightly slower rates of mixture, the fuel and oxidant concentrations which are slightly higher than those obtained with the SCRS model. As a consequence, the NO concentration predictions with the EBU combustion model are generally higher than those obtained with the SCRS model. This is due to the existence of higher concentrations of fuel and oxygen closer to the burner when predictions were performed taking into account the local turbulent scales in the mixing process of the reactants. The SCRS, being faster and as accurate as the EBU model in the predictions of combustion properties appears to be more

*Correspondence to: Viriato Semião, Mechanical Engineering Department, Instituto Superior Tecnico, Av. Rovisco Pais, 1049-001 Lisboa, Portugal
[†]E-mail: viriato@navier.ist.utl.pt
[‡]Research Assistant.
[§]Assistant Professor.
[¶]Full Professor.

Contract/grant sponser: European Collaborative Research JOULE Programme; Contract/grant number: JOE3-CT97-0070

Received 8 August 2000
Accepted 10 January 2001

appropriate. However, should NO be a variable that is predicted, then the EBU model becomes more appropriate. This is due to the better results of oxygen concentration yielded by that model, since it solves a transport equation for the oxidant concentration, which plays a dominant role in the prompt-NO formation rate. Copyright © 2002 John Wiley & Sons, Ltd.

KEY WORDS: turbulent combustion; combustion modelling; gaseous diffusion flames; prompt NO; numerical modelling

1. INTRODUCTION

Combustion and pollution have been virtually inseparable since mankind's discovery of fire. As a result of concerted, worldwide concern during the past two decades, regarding emissions from factory smokestacks and vehicle tailpipes, great strides have been made towards the clean combustion of fuels. The steadily increasing severity of emission regulations has led to much research into the mechanisms of pollutants formation. In addition, limited energy resources and rising fuel prices promoted considerable interest from industrial-intensive users of energy, in supporting the creation of mathematical models that reliably simulate the performance of combustors.

The above-mentioned awareness of the limitation of fossil-fuel resources and the need to comply with increasingly restrictive legislation on pollutant emissions have turned engineers' attention towards the importance of improving industrial combustion equipment design. Consequently, there has been an increase in the quest of new technological developments aiming a cleaner and more efficient combustion.

Traditionally, the design of combustors has been based on the use of empirical models that attempt to correlate the overall performance in terms of simple global parameters such as combustors' volume, inlet air temperature and pressure, mass flow rate and fuel/air ratio. However, a more fundamental approach is needed both for the requirement of energy savings and for the necessity to reduce the emission of pollutants from such systems. Numerical modelling has become a very attractive tool, even indispensable, to combustor designers due to its high flexibility and low cost for the try-out of different geometries and operating conditions, which were made of such codes tools that have been so widely used in the last few years.

The work of Khalil *et al.* (1975) constitutes one of the first milestones as an application of a general numerical procedure to predict combustors' performance. The control volume formulation technique together with the k–ε turbulence model and a flux-model for radiation were used in the calculation procedure. Three different processes, two of them considering a single-step reaction with an infinitely fast rate, simulated the combustion process. In such models, the only transport equation required for the calculation of the participating species was the mixture fraction. These two models differed by the inclusion, or not, of the calculations of the mixture fraction fluctuations. The third model used by the authors considered a finite reaction rate, defined as the minimum value between a kinetic Arrhenius term and a term to evaluate the turbulent mixing rate of the reactants that was proposed by Spalding (1971). Khalil *et al.* (1981) extended the previous work to full-scale boiler predictions.

Gosman *et al.* (1978) studied different burner configurations in a combustor, involving different combustion conditions such as diffusion flames, pre-mixed flames and oxygen-enriched combustion. The authors introduced a probability density function to characterize the instantaneous profile of the mixture fraction so that the model could account for the turbulence

effects in the combustion process. The assumption of a single-step reaction with equal diffusivities for all species was employed, which allowed to linearly relate the species concentrations with the mixture fraction, assuming a defined form for the probability density function (such as the clipped Gaussian or the Beta distributions). A flux-model was used for the radiation. The control volume technique was employed in the solution procedure.

Nikjooy *et al.* (1988) performed predictions for a combustion chamber operating with three different diffusion flames and pre-mixed flames, with and without swirl. A global two-step reaction model for the combustion process was used. The first oxidation reaction generated carbon monoxide and the second one consisted of its oxidation to carbon dioxide. The minimum value between an Arrhenius term and a term expressing the turbulent mixing rate of the reactants was adopted for the combustion modelling. This model required the simultaneous solution of the fuel, the oxidant and the mixture fraction transport equations. The interaction between turbulence and combustion was taken into account by assuming a Beta probability density function for the instantaneous mixture fraction profile.

Carvalho *et al.* (1988a) presented for the first time a three-dimensional calculation of an entire oil-fired glass furnace: the combustion chamber, the glass tank and the batch. For the combustion chamber, the k–ε turbulence model, the simple chemical reacting system (SCRS) of Spalding (1971) for the combustion process and the discrete transfer radiation model together with a soot model to better characterize the flame optical behaviour were used. The authors used the clipped Gaussian distribution to account for the turbulent effects on combustion. The glass tank flow, where buoyancy is the flow-dominant driving force, was modelled taking radiation into account in the energy equation through the use of the optically thick Rosseland approximation. Carvalho *et al.* (1988b) extended the previous work to the evaluation of the influence of the main combustion parameters in the glass furnace operation. The results were considered satisfactory.

Beltagui *et al.* (1991) performed predictions of a burner consisting of 16 radial interfering fuel jets that promoted a high mixing rate of the reactants. This fast mixing of fuel and oxidant close to the burner increased the relative importance of the degree of the reactants' pre-heating and that of the chemical kinetics in the combustion control. In order to account for turbulence and radiation, the authors used, respectively, the k–ε model and the discrete ordinates model. For diffusion flames, the authors used the eddy break-up (EBU) model of Magnussen and Hjertager (1976). For pre-mixing flames, the authors used two different combustion models, the first one frosting the reaction at conditions determined by a critical value of the Damkoler number, whereas the second model made recourse to the extension of the EBU model to pre-mixing flames. The latter establishes that the reaction rate in the fresh-mixture-containing eddies is proportional to the mixing rate with the surrounding hot-products-containing eddies. The high order QUICK scheme was used in the discretization of the convection terms of the transport equations. The pre-mixing flame predictions were considered accurate. Over-predictions of temperature gradients and tangential velocities in the internal recirculation zone (IRZ) were the major flaws reported. These flaws were justified by the use of the single-step global reaction mechanism to model the combustion process.

In the work of Gomes *et al.* (1997), the commercial FLUENT code was used by the authors to evaluate its potential in predicting the combustion process in industrial furnaces, by comparing the predictions against the available experimental data. The computational code used the control volume technique, the k–ε turbulence model and the discrete transfer radiation model. For combustion, the EBU model of Magnussen and Hjertager (1976) together with an

Arrhenius term was used. The predicted temperature field exhibited a good agreement with the experimental data for almost all the physical domain, where the error was below 5%. However, in the near-burner region the model significantly over-predicted the temperature values.

The numerical solution of the time-averaged transport equations together with the k–ε turbulence model and the discrete ordinates radiation model constitute the approach used by Baltasar *et al.* (1997) to predict a laboratory furnace. The combustion was modelled by the SCRS of Spalding (1971). The numerical results exhibited mismatches for the temperature field and species concentrations, particularly, in the near-burner region, which were justified by the poor performance of the k–ε model in predicting swirling flows.

As inferred from the previous works and stated by Borghi (1988), the main difficulties in modelling turbulent diffusion flames arise in the modelling of the kinetics of oxidation reactions and in the interaction between turbulence and combustion. For that reason, many assumptions have been made in order to model the complex phenomena of turbulent diffusion flames. The most common ones are the infinitely fast one-step reaction, the reduced kinetic schemes, the assumed forms for the probability density function and the assumption of the negligible production of turbulence by combustion.

Another flaw in turbulent diffusion flames modelling is the lack of accuracy of the k–ε turbulence model in predicting strong swirling flows. In addition to the above-mentioned physical assumptions, the numerical procedure involved in the use of the control volume technique may exhibit severe inaccuracies. This is the case of the numerical diffusion associated with the adopted integration scheme for the convection and diffusion terms of the transport equations.

In the present work, two different flames induced by different burner geometries are predicted and the results are compared against existing experimental data. Two different combustion models, the SCRS of Spalding (1971) and the EBU of Magnussen and Hjertager (1976) are used and the results are compared in order to assess the importance in combustion modelling of the use of local turbulence scales in the evaluation of the reactants mixture.

Moreover, NO formation in the above-mentioned flames is also analysed. The NO modelling used in the present work comprises the thermal and the prompt routes for NO formation. For the former, the extended Zeldovich mechanism including the reverse reactions (Semião, 1989; Carvalho *et al.*, 1990) is taken into account, while the prompt NO is modelled by an empirical correlation (De Soete, 1974).

2. PHYSICAL AND MATHEMATICAL MODELLING

The two-equation k–ε turbulence model together with the Boussinesq approximation for the Reynolds stresses evaluation is employed herein to close the time-averaged Navier–Stokes equations set. In this model, the eddy viscosity concept is used to calculate the Reynolds stresses and its value is obtained from the solution of the equations for the turbulence kinetic energy, k (Rodi, 1970), and for its dissipation rate, ε (Hanjalic, 1970). In spite of this widely used model described in the open literature, it is well established that its performance is generally poor in the simulation of high-swirling confined flows, particularly in the vicinity of the burner (see, e.g. Rhode *et al.*, 1982). This limitation is due to the inadequate assumption of isotropic viscosity and to the modelling assumptions made in the ε-equation. Some well-known weaknesses and shortcomings of the two-equation k–ε turbulence model are the scalar character of the eddy

viscosity, the inability to reproduce stress anisotropy and the scalar character of turbulence scales. Additionally, the limitations to define a single time or length scale of turbulence to characterize all turbulence interactions, the failure to account for all the physical processes governing the behaviour of ε by virtue of the simplistic form of its basic transport equation, the inadequate incorporation of viscosity damping effects on turbulence structure and the inability and frequently inadequate treatment of boundary conditions, in particular at the solid wall are other flaws of the model. However, its competitiveness in comparison to other turbulence models appears to grow steadily due to the very positive balance between the precision of the yielded results and the computational requirements, particularly for the low-swirling flows with the swirl numbers up to 0.5.

The two main difficulties in the determination of the reaction rate of combustion in engineering equipment are the number of intermediate species participating in the oxidation of hydrocarbons and the highly nonlinear dependence of the reaction rate on temperature.

As for the first above-mentioned difficulty, it is fortunate that for most practical purposes, most of the heat released during the fuel oxidation process can be determined by assuming a single-step global oxidation reaction given by (Gosman *et al.*, 1978): 1 kg [fuel] + s kg [oxidant] $\rightarrow$ (1 + s) kg [products]. Both combustion models used in this work assume such a reaction mechanism, one of them also assuming an infinitely fast reaction rate.

Overcoming the second above-mentioned difficulty is commonly made through the assumption of the oxidation reaction being controlled by turbulent mixing of the different eddies containing the fuel and oxidant, rather than by chemical kinetics (Spalding, 1971; Magnussen and Hjertager, 1976; Gosman *et al.*, 1978; Carvalho *et al.*, 1988a; Baltasar *et al.*, 1997). This approach is used by the second combustion model used herein.

The first model used herein is due to Spalding (1971) and is the well-known SCRS. It assumes a single-step reaction mechanism and also that the diffusivities of all species are equal. Under these circumstances the instantaneous concentrations of the species may be expressed as a function of a single strictly conserved scalar variable, taken in this work as the mixture fraction.

The EBU model, due to Magnussen and Hjertager (1976), assumes the same reaction mechanism as the previous one. Additionally, and according to these authors, this model also assumes that the reactants are homogeneously mixed in the fine-scale dissipative eddies of the turbulent flow. In the limit of fast chemistry, assumption used herein, the reaction rate of the fuel oxidation is controlled by the concentration of the limiting reactant, and by the local turbulence scales given by

$$R_{\mathrm{fu}} = A\rho\frac{\varepsilon}{k}\mathrm{Min}\left[Y_{\mathrm{fu}}, \frac{Y_{\mathrm{ox}}}{s}\right] \tag{1}$$

In addition to the transport equation of fuel, with the source term given by Equation (1), a transport equation for the oxidant is also solved, the source term being given by Equation (2), that makes recourse to similar turbulence and control concepts

$$R_{\mathrm{ox}} = A\rho\frac{\varepsilon}{k}\mathrm{Min}[sY_{\mathrm{fu}}, Y_{\mathrm{ox}}] \tag{2}$$

The general transport equation for all the species concentrations, Y_i, is given by

$$\frac{\partial(\rho u Y_i)}{\partial x} + \frac{1}{r}\frac{\partial(r\rho v Y_i)}{\partial r} = \frac{\partial}{\partial x}\left(\Gamma_{Y_i}\frac{\partial Y_i}{\partial x}\right) + \frac{1}{r\partial r}\left(r\Gamma_{Y_i}\frac{\partial Y_i}{\partial r}\right) + R_{Y_i} \tag{3}$$

where R_{Y_i} is the source term.

Radiation was modelled with recourse to the discrete transfer method of Lockwood and Shah (1981). According to this model, the variation along path ds of the radiant intensity integrated over all the spectral wavelengths is calculated through Equation (4), neglecting the scattering effect. In gaseous flames, the only particulate that can be present is soot. As soot particles contribute almost only to the increase in the flame emissivity, approaching sometimes the black body limit, the assumption of disregarding scattering in gaseous flames is very common (see, e.g. Gomes *et al.*, 1997).

Equation (4) runs thus:

$$\frac{\mathrm{d}I}{\mathrm{d}s} = -kI + \frac{k\sigma T^4}{\pi} \tag{4}$$

In the previous equation, I is the integrated radiant intensity, k is the emission/absorption coefficient, T is the participating media temperature and σ is the Stefan–Boltzmann constant. The first and second right-hand side terms of the previous equation represent, respectively, the radiant energy attenuation due to absorption and the radiant energy augmentation due to emission of the participating media.

The present numerical procedure applies Equation (4) for radiant beams tracked from each wall grid node. This equation is therefore solved within a small number of discretized solid angles of the wall grid point hemispheres, assuming k and T as constant over the finite distance ds travelled by the radiant beam. The absorption coefficient of the participating media, k, was calculated through the model of Truelove (1976).

The radiation boundary conditions for the walls are obtained by energy balances and can be of two types. The first type of boundary condition—prescribed wall temperature at a wall point P, T_W—runs thus (Lockwood and Shah, 1981):

$$q_{-,P} = (1 - \varepsilon_W)q_{+,P} + \varepsilon_W \sigma T_W^4 \tag{5}$$

where $q_{-,P}$ stands for the flux leaving the wall, $q_{+,P}$ stands for the flux arriving at the wall and ε_W is the wall emissivity.

For a point P at a wall with prescribed flux—the second type of boundary condition—the energy balance runs thus (Lockwood and Shah, 1981):

$$q_P = q_{+,P} - q_{-,P} \tag{6}$$

In the previous equation, q_P is the net flux given by

$$q_P = \varepsilon_W q_{+,P} - \varepsilon_W \sigma T_W^4 \tag{7}$$

The concentration of nitric oxide [NO], is calculated by a post-processor routine that solves a transport equation for the NO mass fraction—Equation (3). Two NO formation mechanisms are incorporated in the calculations: the prompt and the thermal mechanisms. The formation of thermal NO takes place through the extended Zeldovich mechanism with the inclusion of the reverse reactions (Semião, 1989 and Carvalho *et al.*, 1992), the rate of formation being given by

$$\frac{\mathrm{d}[\mathrm{NO}]_{\mathrm{th}}}{\mathrm{d}t} = \frac{2[\mathrm{O}]\left(K_1K_2[\mathrm{O}_2][\mathrm{N}_2] - K_{-1}K_{-2}[\mathrm{NO}]^2\right)}{K_2[\mathrm{O}_2] + K_1[\mathrm{NO}]} \tag{8}$$

In the previous equation, K_1, K_2, K_{-1} and K_{-2} are, respectively, the forward and reverse rate constants of the following Zeldovich mechanism reactions:

$$O + N_2 \underset{K_{-1}}{\overset{K_1}{\Leftrightarrow}} NO + N \tag{R1}$$

$$N + O_2 \underset{K_{-2}}{\overset{K_2}{\Leftrightarrow}} NO + O \tag{R2}$$

For the prompt mechanism, an empirical expression similar to that proposed by De Soete (1974) was used. The prompt-NO formation rate is calculated through Equation (9)

$$\frac{d[NO]_{pr}}{dt} = Cf\frac{M^{1+b}}{\rho^{1+b}}[O_2]^b[N_2][\text{fuel}]\exp\left(-\frac{E_a}{R_0 T}\right) \tag{9}$$

where f is a factor dependent on both the number of carbon atoms in the fuel and the fuel air equivalence ratio (Dupont *et al.*, 1993). The constant C was taken as $6.4 \times 10^6\,s^{-1}$ and the reaction order, b, for O_2 was taken as 0.5, as proposed by Weber *et al.* (1995). The activation energy, E_a, was taken as $178\,kJ\,mol^{-1}$ for $T < 1920\,K$ and $303\,kJ\,mol^{-1}$ for $T > 1920\,K$ (Dupont *et al.*, 1993).

3. NUMERICAL SOLUTION PROCEDURE

The numerical solution procedure used in the present work solves the algebraic equations, obtained from the integration of the time-averaged equations expressing the mass, momentum and energy conservation. This integration is performed over the control volumes covering the entire physical domain in such a way that each control volume contains a grid node. Additionally, the integrated versions of the transport equations for scalars describing both turbulence and combustion phenomena are also solved.

Generally, a set of 11 equations is solved. The transported properties are the three velocity components u, v and w, the pressure p, the turbulent quantities k and ε, the mixture fraction f and its variance g, the enthalpy h, and the fuel and oxygen mass concentrations Y_{fu} and Y_{ox}. The cylindrical axisymmetric geometry of the combustor requires the equations to be solved in a cylindrical co-ordinate frame that runs thus:

$$\frac{\partial(\rho u\phi)}{\partial x} + \frac{1}{r}\frac{\partial(r\rho v\phi)}{\partial r} = \frac{\partial}{\partial x}\left(\Gamma_\phi\frac{\partial\phi}{\partial x}\right) + \frac{1}{r}\frac{\partial}{\partial r}\left(r\Gamma_\phi\frac{\partial\phi}{\partial r}\right) + S_\phi \tag{10}$$

In the previous equation, ϕ stands for any of the above-mentioned dependent variables and Γ_ϕ and S_ϕ are the diffusion coefficient and source term of propriety ϕ, respectively. The velocities and pressure are calculated by the SIMPLE algorithm (Patankar, 1980). As presented there, this algorithm involves the solution of the momentum equations using the prevailing pressures, p^*, to yield an intermediate velocity field denoted by u^* and v^*; then velocity corrections by relations of the form $u'_{j,b} = D_n^u(p'_n - p'_P)$, where $D_i^u = \partial u_{j,b}/\partial(p_i - p_P)$, is evaluated from the relevant momentum equation. The previous equation is substituted into the integrated form of the continuity equation to give $a_P p' = \sum_n a_n p' + S_0$ from which p', and hence u' and v', are determined. This equation may be recognized as a form of the Poisson equation for the pressure correction, in which $S_0 = \sum_b \dot{m}_b$ is the local continuity imbalance of the momentum-based u_j^* velocities. Following the solution of this equation, the corrections are

applied by setting $u_j = u_j^* + u_j'$, $p = p^* + p'$, and the entire procedure is repeated until momentum and continuity are both satisfied. The calculations of the remaining dependent variables, as well as the updating of the thermodynamic and transport properties, are incorporated into the above sequence.

The system of algebraic equations resulting from the use of the control volume technique is solved by the tri-diagonal matrix algorithm (TDMA).

As mentioned before, false diffusion may become a plague in the accuracy of the predictions when the flow streamlines are skewed to the grid lines. In order to overcome this problem, the QUICK scheme (Leonard, 1979) is used for the discretization of the diffusion and convection terms of Equation (6) and the results are compared with the hybrid scheme. The QUICK formulation used in this work is that corresponding to the general case of non-uniform grids. The retention of the cross terms in the quadratic function of the QUICK formulation, besides the transversal terms, results in the use of 23 points to estimate the ϕ-fluxes across each control volume interfaces as opposed to the 5 points used by the hybrid scheme.

4. RESULTS AND DISCUSSION

In order to validate the models described before, predictions are performed for the laboratory furnace sketched in Figure 1 and the results are compared herein against the available experimental data. The furnace consists of a cylindrical combustion chamber composed of five steel segments, each with 0.2 m height and 0.3 m of internal diameter. One of the segments has four rectangular ports for probing and viewing which are closed with quartz or steel inserts as described by Baltasar *et al.* (1997).

The experimental data used for validation purposes (Baltasar *et al.*, 1997; Ruao *et al.*, 1999) are referred to the same furnace fired with two different burners inducing distinct flow configurations and flame structures.

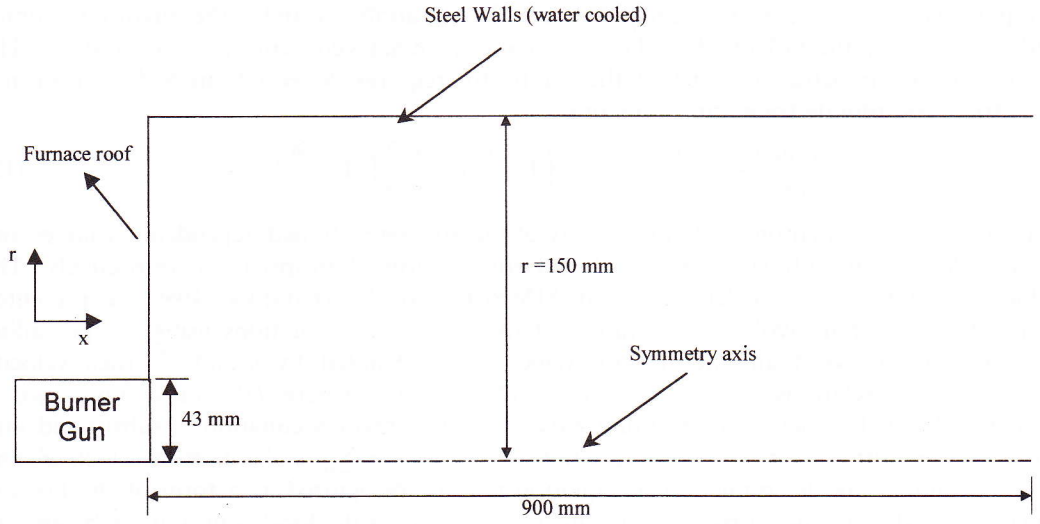

Figure 1. Scheme of the laboratory furnace used for predictions.

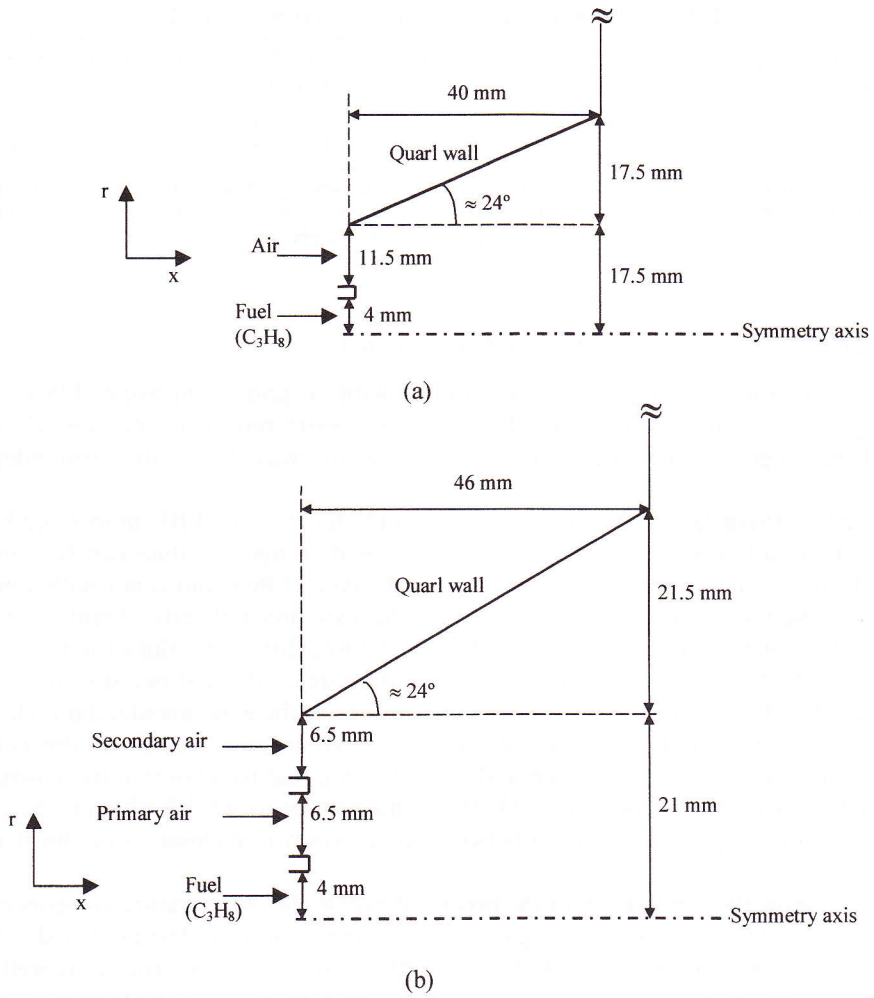

Figure 2. Sketch of burners' geometries: (a) Burner A, (b) burner B.

As described by Baltasar *et al.* (1997), the first burner geometry (hereafter burner A), is shown in Figure 2(a) and is typical of that used in power stations for wall-fired boilers. It consists of a burner gun (i.d. 8 mm, o.d. 12 mm) and a secondary air supply in a conventional double-concentric configuration terminating in a quarl of 24° half-angle and a length-to-diameter ratio of ≈ 1. The experimental conditions simulated in the present work correspond to flame B1 of Baltasar *et al.* (1997) and are summarized in Table I.

The second burner geometry (hereafter burner B), shown in Figure 2(b), also consists of a burner gun (i.d. 8 mm, o.d. 12 mm) and an air supply in a conventional concentric configuration. However, the air is supplied in two separated streams, both crossing very thin guide vanes to induce rotation to the flow–swirl. The experimental conditions simulated in this work correspond to flame P6 of Ruao *et al.* (1999) which are summarized in Table I.

Table I. Experimental conditions for burners A and B.

	m_{ox}(1) (Kg s^{-1})	u_{ox} (2) (m s^{-1})	u_{oxP} (3) (m s^{-1})	u_{oxS} (4) (m s^{-1})	λ(5)	m_f (6) (kg s^{-1})	u_f (7) (m s^{-1})	T_f (8) (°C)	T_{ox} (9) (°C)	S_{ox} (10)	S_{oxP}(11)	S_{oxS}(12)
Burner A	5.2	5.0	—	—	1.07	3.1×10^{-4}	3.32	20	20	0.5	—	—
Burner B	—	—	2.42	5.46	1.07	—	3.58	20	20	—	1	0.3

Note: (1) Air mass flow rate, (2) air inlet velocity, (3) primary air inlet velocity, (4) secondary air inlet velocity, (5) excess air ratio, (6) fuel mass flow rate, (7) fuel inlet velocity, (8) fuel inlet temperature, (9) air inlet temperature, (10) air swirl number, (11) primary air swirl number, and (12) secondary air swirl number.

4.1. Flow and combustion predictions—models validation

The predictions for burner A were performed with a grid comprising 138×79 nodes, respectively, in the x and r directions, that was made more refined in the zone closer to the burner, where the gradients are more pronounced. The grid was chosen after grid independence tests.

As referred by Brizuela and Bilger (1996), the parameter A of the EBU model, see Equations (1) and (2), is usually taken as constant, but quite a wide range of values can be found in the literature. In reality, the optimal value depends on the type of flow and is normally obtained by fitting the predictions of fuel concentrations to the experimental data. Figure 3 shows the predicted values of fuel concentration profiles using three different values for the constant A ($A = 0.5$, 1.0 and 3.0). As it can be observed from this figure, at the first two stations ($x = 54$ and 84 mm) the value $A = 3.0$ produced the highest deviations to the experimental data. However, at the following three stations ($x = 164$, 249 and $x = 369$ mm), this value for the constant A produced results closer to the experimental data, indicating that the choice of this constant value is not straightforward. In the present work, this value was set to $A = 1.0$ which is the value that produces the best compromise solution between the reaction rate closer to the burner and the flame length.

Figures 4–7 show the comparison of the predicted profiles for temperature and concentrations of fuel, oxygen and CO_2, respectively, against the experimental data. The predicted values were obtained with recourse to both the SCRS and EBU models for combustion, as well as using both the numerical discretisation schemes for the convection terms of the transport equations: the hybrid scheme and the QUICK scheme.

For the temperature, at the first station ($x = 42$ mm, Figure 4), both combustion models reflect the physical features of the experimental data, namely the deep decay of temperature due to the cooling effect of the oxidant stream ($r \approx 50$ mm). However, both models over-predict the temperature in the symmetry axis and underestimate the radius at which the flame front is located (the peak value of the temperature profile). These mismatches are related to those appearing in the species concentration predictions. Indeed, as it can be seen from Figures 5–7 both models underestimate the fuel and the oxidant concentrations at the near-burner region ($r < 50$ mm) and over-predict the CO_2 concentration at the same zone. From this, one may conclude that both models predict higher reaction rates than the real ones. Moreover, the above-described differences observed could also be due to a more intense CO_2 recirculation predicted by the turbulence model that might cause a dilution effect on the other species.

In order to perform a more conclusive analysis, experimental data for velocities would be required. In the absence of such data, recourse is made for predictions to perform such an

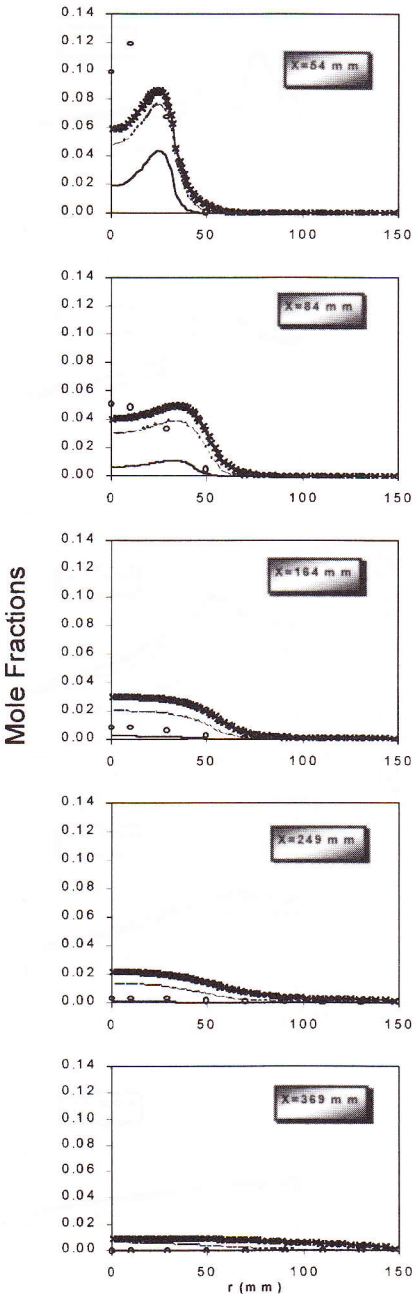

Figure 3. Fuel concentration profiles (mole fractions) for burner A: predictions with different values of parameter A and experimental values. —×— ($A = 0.5$); - - - - - - ($A = 1.0$); —— ($A = 3.0$); ○, measurements.

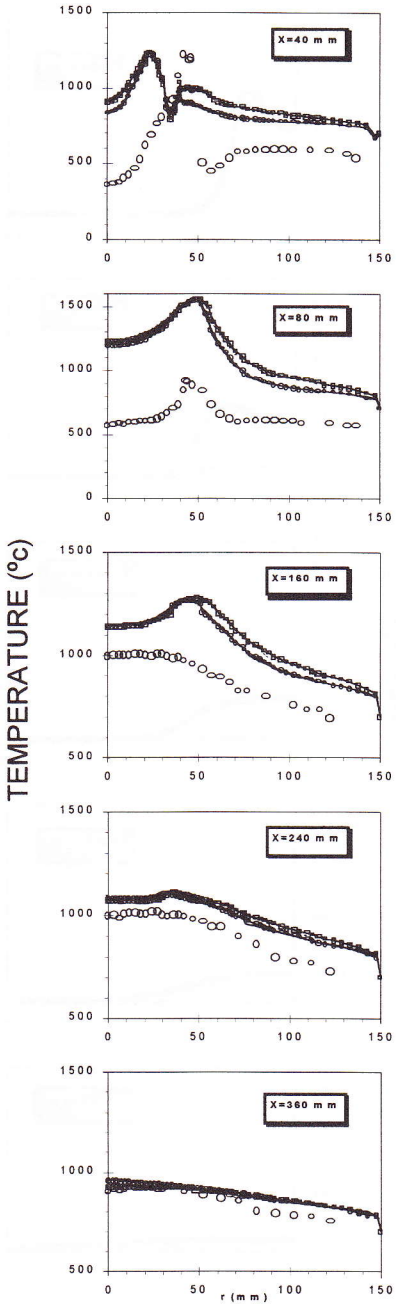

Figure 4. Temperature profiles for burner A: experimental values and predicted values. ------, EBU + hybrid; —□—, SCRS + hybrid; ——, EBU + QUICK; —○—, SCRS + QUICK; ○, measurements.

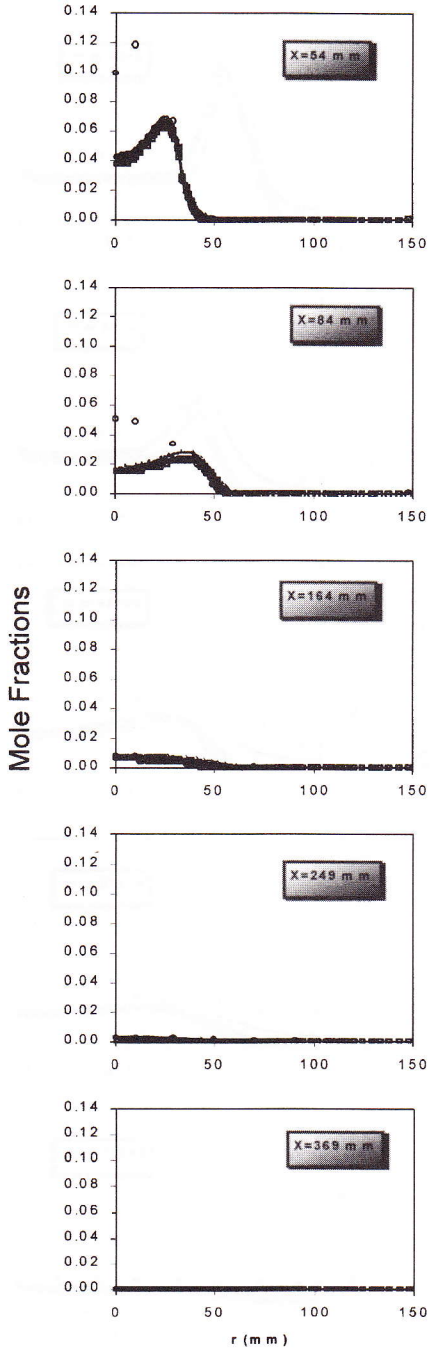

Figure 5. Fuel concentration profiles (molar fractions) for burner A: experimental values and predicted values. ------, EBU + hybrid; —□—, SCRS + hybrid; ——, EBU + QUICK; —○—, SCRS + QUICK; ○, measurements.

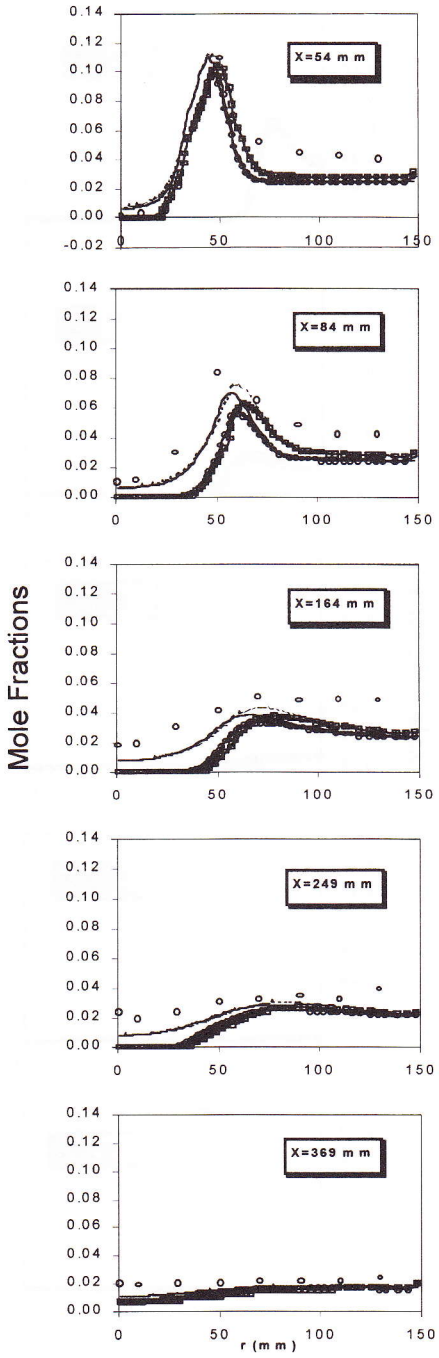

Figure 6. Oxidant concentration profiles (molar fractions) for burner A: experimental values and predicted values. ------, EBU + hybrid; —□—, SCRS + hybrid; ——, EBU + QUICK; —○—, SCRS + QUICK; ○, measurements.

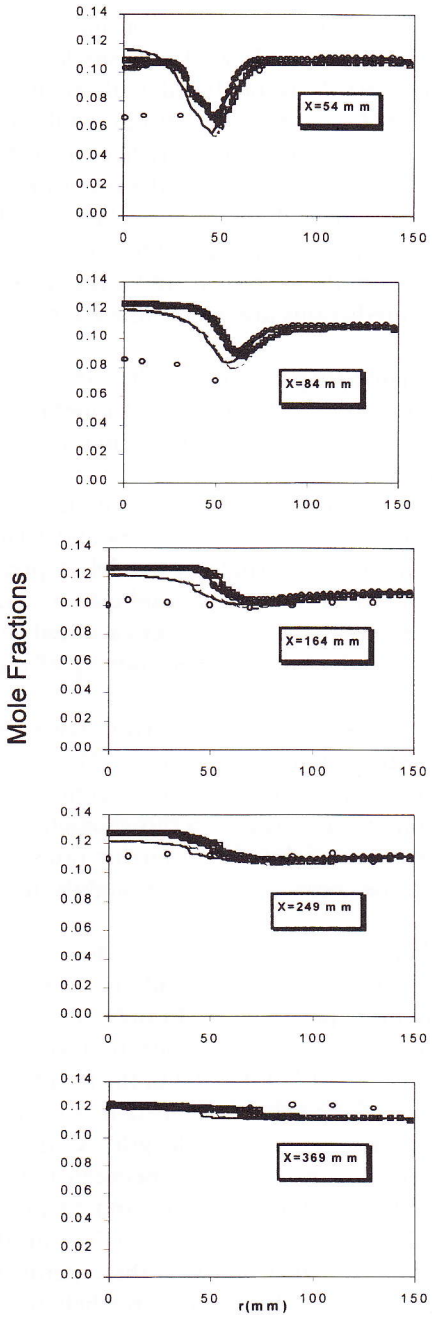

Figure 7. CO_2 concentration profiles (molar fraction) for burner A: experimental values and predicted values. ------, EBU + hybrid; —□—, SCRS + hybrid; ——, EBU + QUICK; —○—, SCRS + QUICK; ○, measurements.

analysis. Figure 8 shows the predicted axial velocity profiles. As it can be observed, both the hybrid and the QUICK schemes predict an IRZ of very similar lengths ($\approx$ 150 mm). However, the external recirculation zone (ERZ) is predicted with slightly different lengths by those schemes: QUICK predicts an ERZ length of $\approx$ 400 mm, while the hybrid scheme predicts an ERZ length of 350 mm. The similitude in the flow predictions using both the above-mentioned schemes yields the similitude of the temperature and the species-predicted profiles (Figures 4–7). Away from the symmetry axis, the radial decrease of oxidant and the radial increase of CO_2 are in agreement with the experimental data (Figures 6 and 7).

At the second station ($x = 80$ mm), numerical and experimental temperature profiles are qualitatively similar, albeit the predictions are overestimated, particularly inside the flame front ($r < 50$ mm).

The predicted value of the flame length is higher than the real one, as it can be seen from Figure 4 at $x = 160$ mm. At this station, the predicted temperature profiles still exhibit a peak indicating the chemical reaction zone, while the experimental profile is flatter, indicating that the models underestimated the reaction rates.

The discrepancies observed between the experimental and the numerical fuel profiles closer to the burner and to the symmetry axis (Figure 5 at $x = 54$ and 84 mm) are due to two reasons. First, the known limitations of the k–ε turbulence model in predicting the confined swirling flows are applied to this case, where air enters the combustion chamber with a swirl number of 0.5. Secondly, the combustion model does not take into account the kinetics of combustion. As in this region, one may expect very intense turbulent mixing of the reactants, this can turn the reaction control to kinetics.

From all the previous results, it is clear that away from the burner region, both combustion models (SCRS and EBU) produce similar predictions. This is due to the high mixing rate between the reactants occurring in the near-burner region, that makes the SCRS a good approximation to model the combustion process in this geometry. However, closer to the burner ($x < 84$ mm), the EBU model predicts slightly lower mixing rates, as it can be observed from the fuel concentration values at those locations that are slightly higher than those predicted by the SCRS.

As for burner B, the predictions were performed with a grid comprising 105×85 nodes, respectively, in the x and r directions, that was made more refined in the zone closer to the burner where the gradients are more pronounced. In order to choose the best value of constant A of Equations (1) and (2), predictions of fuel concentration were performed using three distinct values for the referred parameter, $A = 0.5$, 1.0 and 3.0, the results being represented in Figure 9. As already described, the choice of the value for constant A is made as a compromise between the reaction rate near the burner and the flame length. At the first station ($x = 46$ mm), the reaction rate is under-predicted and the difference between the three constants is practically non-existent. At the second and third stations ($x = 67$ and 88 mm), the value $A = 3.0$ yields the worst results when compared to the measurements, while at the last two stations this is the constant value that predicts with higher precision the experimental values. In this work, the value $A = 3.0$ was chosen because this is the one that predicts the flame length better.

Figures 10 and 11 depict the comparison between the predictions and the measurements of the radial profiles, respectively, for the temperature and the fuel concentration, at the axial stations at which measurements were available. As the global thermal conditions for burner B are similar to those for burner A, namely the thermal power input (14.4 kW for burner A and 15 kW for burner B), the excess air ratio (1.07 for both cases) and the inlet reactants temperatures (20°C

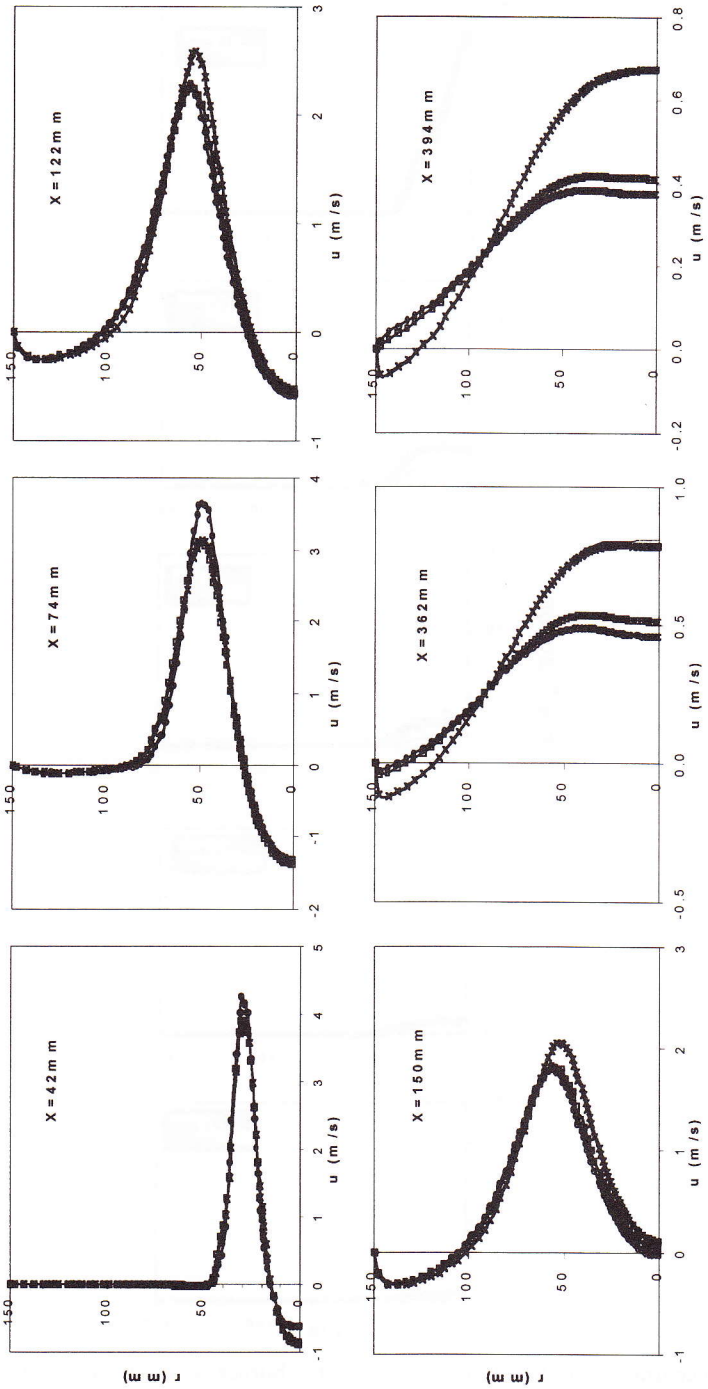

Figure 8. Axial velocity profiles: predicted values. —×—, EBU + hybrid; —□—, SCRS + hybrid; ——, EBU + QUICK; —○—, SCRS + QUICK;

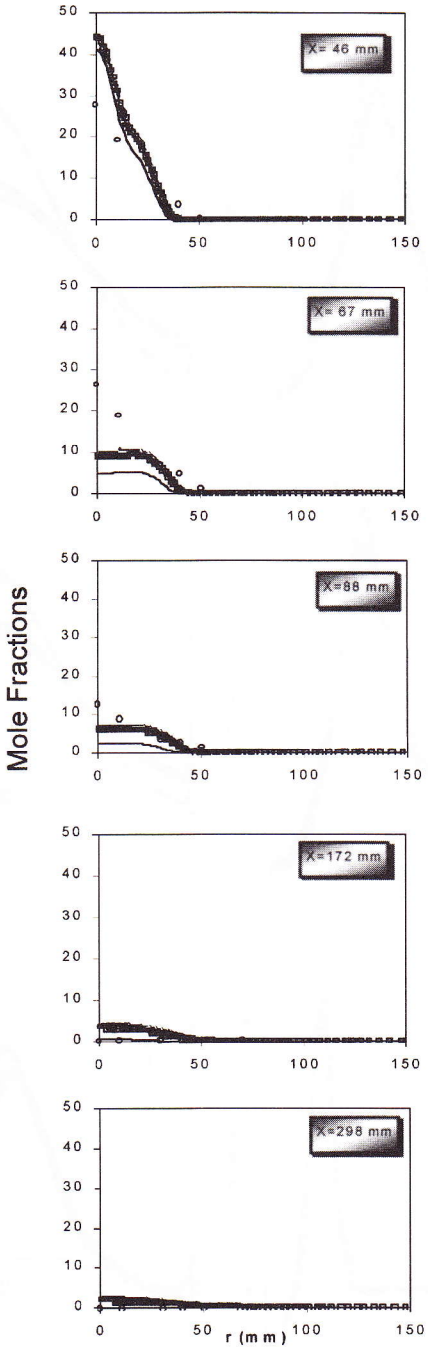

Figure 9. Fuel concentration profiles (mole fractions) for burner A: predictions with different values of parameter A and experimental values. - - - - - - ($A = 0.5$); —□— ($A = 1.0$); —— ($A = 3.0$); ○, measurements.

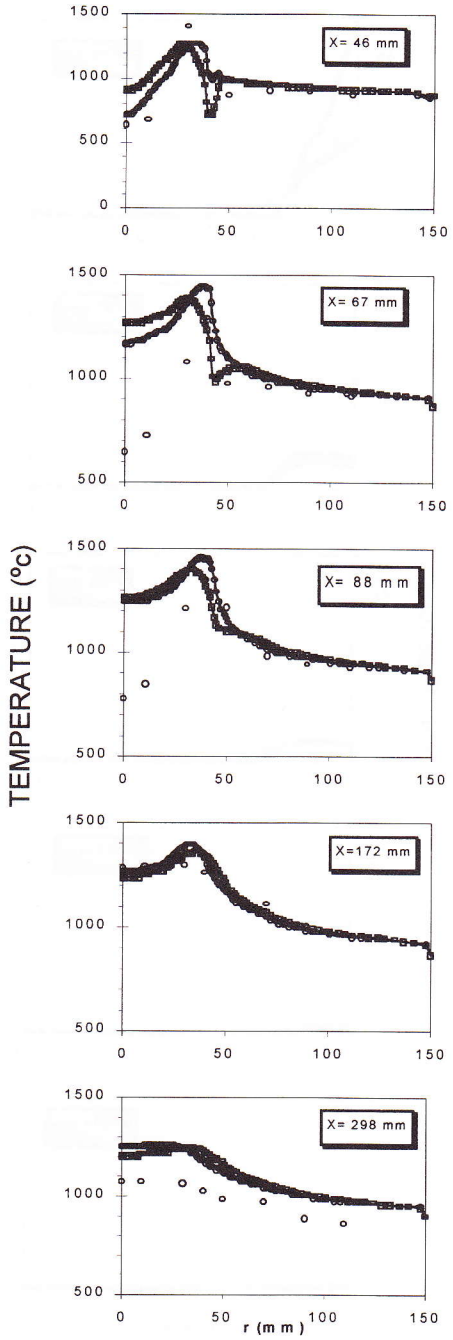

Figure 10. Temperature profiles for burner B: experimental values and predicted values. ------, EBU + hybrid; —□—, SCRS + hybrid; ——, EBU + QUICK; —○—, SCRS + QUICK; ○, measurements.

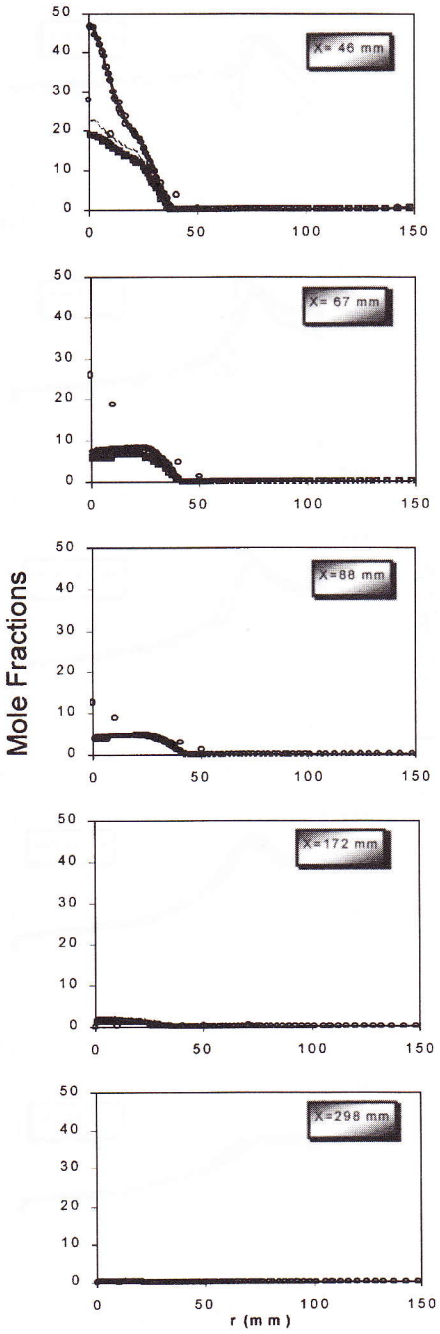

Figure 11. Fuel concentration profiles (mole fractions) for burner B: experimental values and predicted values. ------, EBU + hybrid; —□—, SCRS + hybrid; ——, EBU + QUICK; —○—, SCRS + QUICK; ○, measurements.

for both cases), an evaluation of the differences between the two models' results will be performed keeping in mind that the burners induce distinct flow configurations.

Comparing Figures 5 and 11, it is clear that burner B induces a smaller combustion reaction rate closer to the burner, as there is a smaller decrease of the fuel concentration from the first to the second station. However, further downstream, this reaction rate for burner B increases in such a way that the flame length is similar for both burners. The distinct flow field induced by the two burners explains these differences. Figure 12 shows the predicted radial profiles of the axial component velocity obtained with both the QUICK and the hybrid schemes and with the SCRS combustion model. For comparison purposes, the same velocity profiles for burner A predicted with the QUICK scheme and the SCRS combustion model is also represented in that figure. From this figure it can be concluded that burner A yields a longer and wider IRZ (see station $x = 74$ and 122 mm). To this wider recirculation zone, a stronger radial deflexion of the fuel jet corresponds and consequently, a more intense rate of fuel and oxidant mixing in the region closer to the burner, which explains the higher rate of combustion for burner A.

The more pronounced differences between the species concentrations yielded by the QUICK and the hybrid schemes, compared with the smaller differences in the case of burner A, emerge from the differences in the predicted values of the flow field by the two schemes (see Figure 12). Due to the geometry of burner B, exhibiting two distinct air inlets with different swirl numbers, a more pronounced skewness between the streamlines and the numerical grid arises, which promotes the appearance of false diffusion in the predictions yielded by the hybrid scheme.

Conclusions similar to those drawn for burner A away from the near-burner region, as far as the SCRS accuracy is concerned, are also applied to the case of burner B. Indeed, the predictions indicate that near the burner the mixing between fuel and oxidant is very intense. This means that the local turbulence scales of both flows are such that the mixture between fuel-containing eddies and oxygen-containing eddies occur almost instantaneously and immediately after they get into contact—note that the fuel and oxidant are introduced separately into the combustion chamber. Therefore, SCRS appears to be appropriate for combustion predictions as it is faster and as accurate as the EBU model.

4.2. NO_x predictions and validation

Figure 13 shows the experimental and predicted NO profiles for burner A. As reported by Baltasar *et al.* (1997) the dominant route of NO formation in the furnace under study is the prompt mechanism. Figure 14 shows the NO concentration predictions using the prompt mechanism as the only NO source against predictions using both the prompt and the thermal mechanisms as NO sources, performed with the QUICK scheme. As it can be observed, the differences are imperceptible, except very small ones at the station located at $x = 84$ mm, which can be explained by the high temperature level predicted in that region (Figure 4, at $x = 80$ mm). The prompt route control of the NO formation is confirmed by the experimental results trend, which show that at the first two near-burner stations NO exhibits very high concentrations, decreasing sharply in the downstream axial direction until it reaches a radial uniform concentration of around 38 ppm. As established by Equation (8), the prompt-NO formation depends both on fuel and oxidant concentrations. The under-predicted values with the SCRS model at the first station ($x = 54$ mm) are explained by the under-predicted values of fuel concentration in that region yielded by this model (see Figure 5). The slightly better results obtained with the EBU model for the same station are also related with the slightly better results

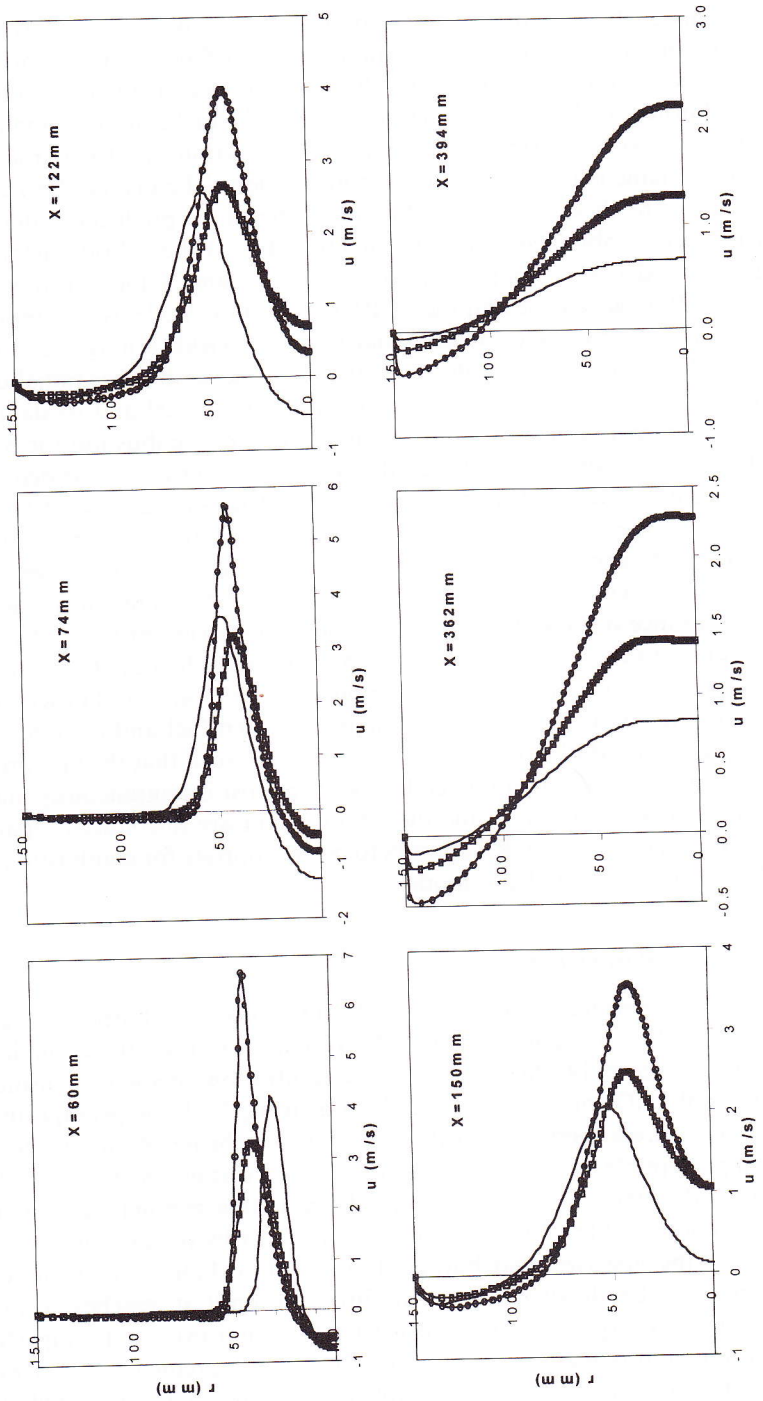

Figure 12. Axial velocity profiles: predicted values. —□—, SCRS + hybrid; (burner B); —○—, SCRS + QUICK (burner B) ——, SCRS + QUICK; (burner A).

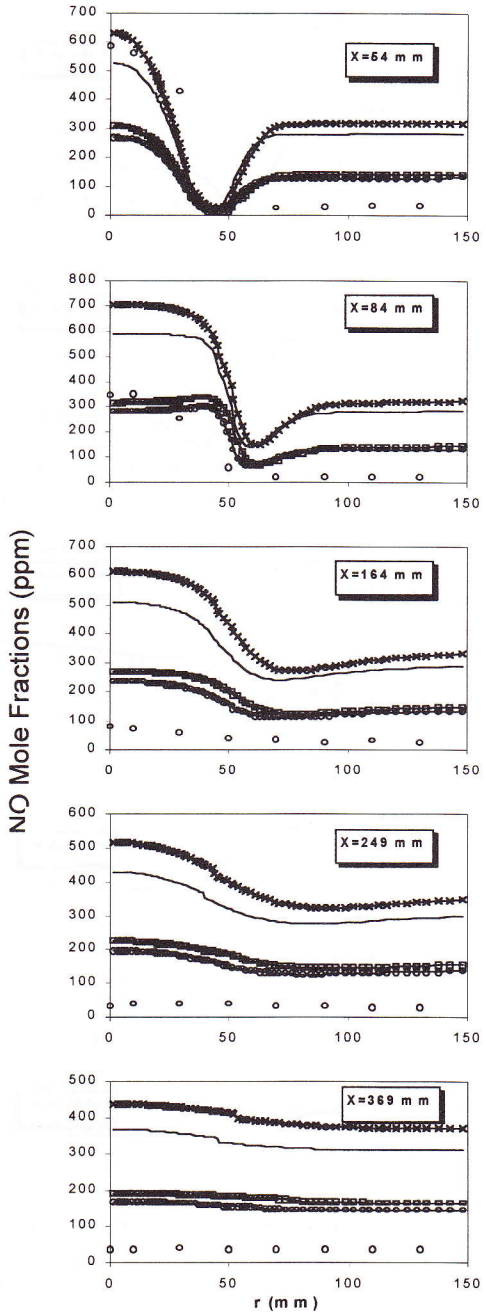

Figure 13. NO concentration profiles (molar fractions) for burner A: experimental values and predicted values. —×—, EBU + hybrid; —□—, SCRS + hybrid; ——, EBU + QUICK; —○—, SCRS + QUICK; ○, measurements.

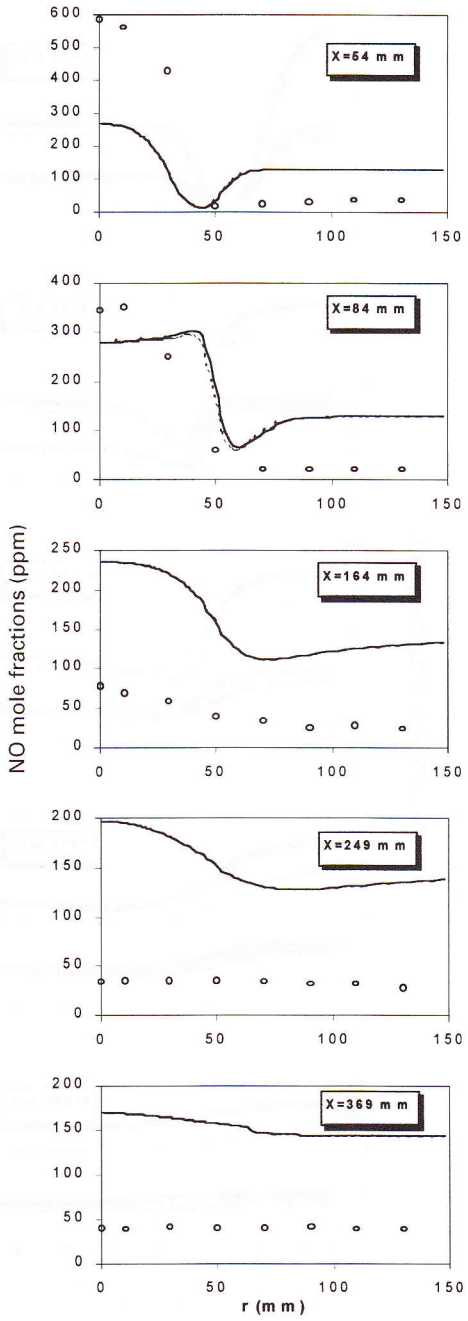

Figure 14. NO concentration profiles (molar fractions) for burner A: prompt-NO mechanism and thermal-NO mechanism. ——, Thermal + prompt; ....., prompt.

of oxidant concentration yielded by that model (see Figure 6, $x = 54$ mm). The predicted decrease of NO in the axial direction, slower than that revealed by the measurements, is explained by the slower decrease for the fuel concentration, previously reported.

Figure 15 compares, for burner B, the predicted NO concentration profiles against the corresponding measured values. As reported by Ruao *et al.* (1999), the dominant NO formation mechanism in their experiments is once more the prompt route. The predictions revealed that the contribution of the thermal mechanism for the total NO formation was negligible. The mismatches observed for the fuel predictions have consequent errors in the NO predictions. Indeed, the NO under-predicted values closer to the burner ($x = 46$ and 67 mm) are a direct consequence of the under-predicted fuel concentration values at those stations (see Figure 11). Additionally, over-predicted values of NO concentration at the two last stations ($x = 172$ and 298 mm) are a direct consequence of the over-predicted fuel concentration (see Figure 11).

If NO is a variable to be predicted, the EBU model becomes more appropriate. This emerges from the better results of oxygen concentration yielded by that model, since it solves an oxidant transport equation, while the oxidant concentration values play a dominant role in the prompt-NO formation rate.

5. CONCLUSIONS

A numerical model, based on control volume formulation technique, for the prediction of the turbulent flow, combustion, thermal radiation and pollutants formation in diffusion flames was presented and validated against experimental data. Two different turbulent-mixing models for combustion, the simple chemical reacting system (SCRS) and the eddy break-up (EBU), were compared in order to assess the need to make recourse to local turbulent scales to evaluate the reactants' mixing rate. Predictions performed for a gaseous-fuelled combustor fired with two different burners, that induced different aerodynamic conditions inside the combustion chamber, exhibited a good agreement with the experiments.

Besides combustion properties, NO predictions were also performed by a prompt-NO formation model together with a thermal-NO formation model, used as a post-processor routine. The results were generally in good agreement with the experimental values.

The models used in this work were, therefore, able to predict the main features of the studied flames. However, in the region closer to the burner some less accurate results were yielded by the models results. This can be explained by the two factors, the first being the well-known shortcomings of the k–ε turbulence model in predicting highly swirling flows. The second factor is related to the use of combustion models not taking into account the chemical kinetics that can control the combustion process in the burner region whenever the mixing process becomes too fast.

The predictions revealed that the mixture between the reactants occurred very close to the burner and almost instantaneously, that is, immediately after the fuel-containing eddies came into contact with the oxidant-containing eddies. As a result, away from the burner, the SCRS model, that assumes an infinitely fast mixing rate, appeared to be as accurate as the EBU model. Closer to the burner, however, the EBU model, which makes the reactants' mixing rate dependent on both the local turbulent scales and on the reactants' concentrations, yielded slightly slower rates of mixture. This was observed from the fuel and oxidant concentrations

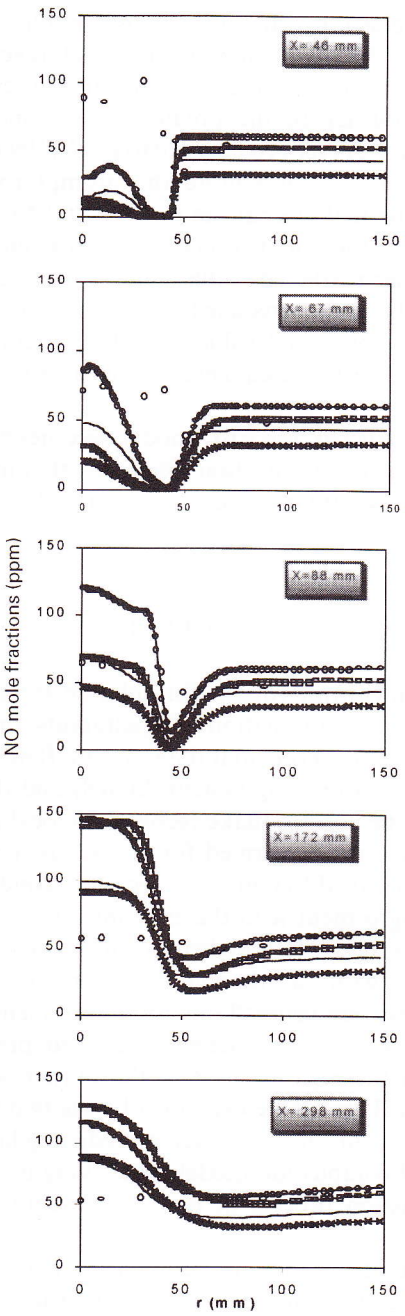

Figure 15. Comparison between measured and predicted radial profiles of NO mole fraction for burner B. —×—, EBU + hybrid; —□—, SCRS + hybrid; ——, EBU + QUICK; —○—, SCRS + QUICK; ○, measurements.

that were slightly higher than those obtained with the SCRS model. As a consequence, the NO concentration predictions obtained with the EBU model were generally higher than those obtained with the SCRS model. This was explained by the existence of higher concentrations of fuel and oxygen closer to the burner, when predictions were performed taking into account the local turbulent scales in the mixing process of the reactants. The SCRS, being faster and as accurate as the EBU model in the predictions of combustion properties proved to be, for the present geometries, more appropriate. However, should NO be a variable that is predicted, then the EBU model becomes more appropriate. This emerged from the better results of oxygen concentration yielded by that model, since it solved an oxidant transport equation, which played a dominant role in the prompt-NO formation rate.

ACKNOWLEDGEMENTS

This work has been partially performed with the financial support of the European Collaborative Research JOULE Programme, under the contract JOE3-CT97-0070.

NOMENCLATURE

A = constant of the EBU model
b = reaction order for oxygen
C = constant of the prompt-NO model
E_a = activation energy (kJ mol^{-1})
f = factor in the prompt-NO model
I = radiant energy intensity
K = equilibrium constant (cm^3 $mole^{-1}$ s^{-1})
k = turbulent kinetic energy
m = mass flow rate (kg s^{-1})
M_j = molecular weight of j species
R_i = reaction rate of i species (kg.s^{-1})
R_0 = universal gas constant
S = swirl number
S_ϕ = source term of propriety ϕ
s = stoichiometric coefficient
T = temperature (K)
u = axial velocity (m s^{-1})
v = radial velocity (m s^{-1})
Y_i = mass fraction of i species
ϕ = generic property
Γ_ϕ = diffusion coefficient of the property ϕ
σ = stefan–Boltzmann constant
λ = excess air ratio
ρ = density (kg m^{-3})

Subscripts
fu = fuel
ox = oxidant

P = primary air
pr = prompt-NO mechanism
S = secondary air

REFERENCES

Baltasar J, Carvalho MG, Coelho P, Costa M. 1997. Flue gas recirculation in a gas-fired laboratory furnace: measurements and modelling. *Fuel* **76**:919.

Beltagui SA, Stopford PJ, Fuggle RN, Kenbar AMA, Ralston T, Marriot N. 1991. Modelling gas-fixed furnace flow and combustion using the PCOC code. Eurotech-Direct Conference (C413/054).

Borghi R. 1988. Turbulent combustion modelling. *Progress in Energy and Combustion Science* **14**:245.

Brizuela EA, Bilger RW. 1996. On the Eddy break-up coefficient, brief communication. *Combustion and Flame* **104**:208.

Carvalho MG, Oliveira P, Semião V. 1988a. A three dimensional modelling of an industrial glass furnace. *Journal of the Institute of Energy* **LXI**:143.

Carvalho MG, Oliveira P, Semião V. 1988b. Modeling and optimization of an industrial glass furnace. *AIAA Progress in Astronautics and Aeronautics* **113**:363.

Carvalho MG, Semião VS, Lockwood FC, Papadopoulos C. 1990. Predictions of nitric oxide emissions from an industrial glass melting furnace. *Journal of the Institute of Energy* **LXIII**:47.

Carvalho MG, Semião VS, Coelho PJ. 1992. Modelling and optimization of the NO formation in an industrial glass furnace. *ASME Journal of Engineering for Industry* **114**:514.

De Soete GG. 1974. Overall reaction rates of NO and N_2 formation from fuel nitrogen. *15th Symposium (International) on Combustion*. The Combustion Institute: Pittsburg, PA, 1093.

Dupont V, Pourkashanian M, Williams A. 1993. Modelling of process heaters fired by natural gas. *Journal of the Institute of Energy* **LXVI**:20.

Gomes MSP, Nieckele AO, Naccache MF, Kobayashi WT. 1997. Numerical investigation of the enriched combustion process in a cylindrical furnace. *4th International Conference on Technologies and Combustion For a Clean Environment*, Vol. II, 36.1.

Gosman AD, Lockwood FC, Salooja AP. 1978. The prediction of cylindrical furnaces gaseous fuelled with premixed and diffusion burners. *17th Symposium (International) on Combustion*. The Combustion Institute: Pittsburg, PA, 747.

Hanjalic K. 1970. Two dimensional axisymmetric turbulent flow in ducts. *Ph.D. Thesis*, Mechanical Engineering Department, Imperial College of Science and Technology, London.

Khalil EE, Spalding DB, Whitelaw JH. 1975. The calculations of local flow properties in two-dimensional furnaces. *International Journal of Heat and Mass Transfer* **18**:775.

Khalil EE, Hutchinson P, Whitelaw JH. 1981. The calculation of the flow and heat-transfer characteristics of gas-fired furnaces. *18th Symposium (International) on Combustion*. The Combustion Institute: Pittsburg, PA, 1927.

Leonard BP. 1979. A stable and accurate convection modelling based in quadratic upstream interpolation. *Computer Methods in Applied Mechanics and Engineering* **19**:59.

Lockwood FC, Shah NG. 1981. A new radiation solution method for incorporating in general combustion prediction procedures. *18th Symposium (International) on Combustion*. The Combustion Institute: Pittsburg, PA, 1405.

Magnussen BF, Hjertager BH. 1976. On mathematical modelling of turbulent combustion with special emphasis on soot formation and combustion. *16th Symposium (International) on Combustion*. The Combustion Institute: Pittsburg, PA, 719.

Nikjooy M, So RMC, Peck RE. 1988. Modelling of jet- and swirl-stabilized reacting flows in axisymmetric combustors. *Combustion Science and Technology* **58**:135.

Patankar SV. 1980. *Numerical Heat Transfer and Fluid Flow*. Hemisphere Publishing Corporation: New York.

Rodi W. 1970. Basic equations for turbulent flow in Cartesian and cylindrical co-ordinates. *Internal Report BL/TN/A/36*, Mechanical Engineering Department, Imperial College of Science and Technology, London.

Ruao M, Costa M, Carvalho MG. 1999. A NO_x diagnostic system based on a spectral ultraviolet/visible imaging device. *Fuel* **78**:1283.

Semião VS. 1989. Modelação da combustão, transferência de calor e emissão de poluentes em sistemas de queima de combustíveis liquidos. *Ph.D. Thesis*, Departamento de Engenharia Mecanica, Instituto Superior Tecnico, Universidade Tecnica de Lisboa (in Portuguese).

Rhode DL, Lilley DG, Mclaughlin DK. 1982. On the predictions of swirling flow-fields found in axisymmetric combustor geometries. *Transactions of ASME: Journal of Fluids Engineering* **104**:378.

Spalding DB. 1971. Mixing and chemical reaction in steady confined turbulent flame. *13th Symposium (International) on Combustion*. The Combustion Institute: Pittsburg, PA, 649.

Truelove JS. 1976. A mixed grey gas model for flame radiation. *AERE Harwell Report No. HL*76/3448/*KE*, Harwell, England.

Weber R, Peters A, Breithampt P, Visser B. 1995. Mathematical modeling of swirling flames of pulverized coal: what can combustion engineers expect from modeling? *Journal of Fluids Engineering* **117**:289.